ACS APPLIED MATERIALS & INTERFACES

Research Article

www.acsami.org

Self-Assembly Fabrication of Hollow Mesoporous Silica@Co−Al Layered Double Hydroxide@Graphene and Application in Toxic Effluents Elimination

Shu-Dong Jiang,[†] Lei Song,[†] Wen-Ru Zeng,[†] Zheng-Qi Huang,[†] Jing Zhan,[†] Anna A. Stec,[§] T. Richard Hull,[§] Yuan Hu,*[,†,‡] and Wei-Zhao Hu*[,†]

[†]State Key Laboratory of Fire Science, University of Science and Technology of China, 96 Jinzhai Road, Hefei, Anhui 230026, People's Republic of China

[‡]Suzhou Key Laboratory of Urban Public Safety, Suzhou Institute for Advanced Study, University of Science and Technology of China, 166 Ren'ai Road, Suzhou, Jiangsu 215123, People's Republic of China

[§]Centre for Fire and Hazards Science, University of Central Lancashire, Preston PR1 2HE, United Kingdom

Supporting Information

ABSTRACT: Here, we propose a self-assembly process to prepare hierarchical HM-SiO_2@Co−Al LDH@graphene, with the purpose of combining their outstanding performance. Hollow mesoporous silica was first synthesized as the core, using a novel sonochemical method, followed by a controlled shell coating process and chemical reduction. As a result of the electrostatic potential difference among HM-SiO_2, Co−Al LDH, and graphene oxide, the HM-SiO_2 spheres were coated by Co−Al LDH and graphene. Subsequently, the HM-SiO_2@Co−Al LDH@graphene spheres were introduced into an epoxy resin (EP) matrix for investigation of their toxic effluents capture and elimination effectiveness during combustion. The amount of toxic CO and volatile organic compounds from the epoxy resin decomposition significantly suppressed after incorporating the HM-SiO_2@Co−Al LDH@graphene hybrids, implying a reduced toxicity.

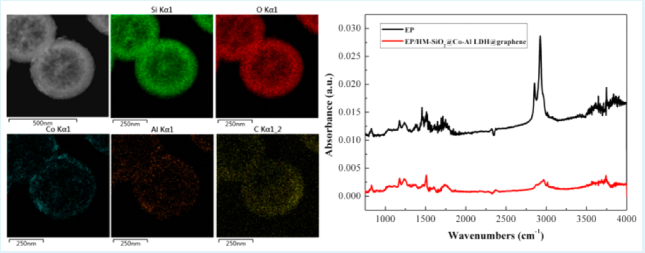

KEYWORDS: *HM-SiO_2@Co−Al LDH@graphene, self-assembly, epoxy, composites, fire effluents elimination, mechanism*

1. INTRODUCTION

As a general thermoset plastic, epoxy resin (EP) is extensively used in adhesive, potting, and coating areas, because of its dimensional stability and excellent mechanical performance.[1] However, its high flammability greatly limits its application in some fields. Especially, inhalation of fire effluents is the major cause of death or permanent injury in fire accidents.[2−4] Therefore, efficient removal of toxic effluents released during combustion will be significant for saving lives and health issues in real fires.

For this promise to be realized, hollow mesoporous silica (HM-SiO_2) has emerged, as a consequence of their fascinating applications in adsorption and catalysis, as adsorbents, catalysts, and catalyst supports.[5−7] Until now, numerous efforts have been devoted to prepare HM-SiO_2 including conventional soft and hard template methods.[6,8−12] However, the preparation and removal procedures of the templates are generally complicated, uneconomical, and time-consuming. Therefore, one of the main scientific challenges to be achieved in the field of HM-SiO_2 research should be to develop a facile and effective strategy for preparing the hollow structures. Meanwhile, it is highly urgent to maximize the performance of HM-SiO_2 toward the capture and elimination of harmful gases. Recently, combining materials with different functions to form hybrid and hierarchical structures is an effective approach toward novel design and high performance.[13−16] Li et al. prepared the multifunctional dual-compartment Janus mesoporous silica nanocomposites of UCNP@SiO_2@mSiO_2&PMO through a novel anisotropic island nucleation and growth approach with the ordered mesostructure.[17] A novel Fe_3O_4@SiO_2@NiAl-LDH catalyst was synthesized for the practical purification of recombinant proteins.[18] As far as we know, transition metals especially cobalt were proved to be an effective catalyst for toxic gases elimination.[19,20] Also, it has been reported that a Co_3O_4/graphene hybrid shows a synergistic catalyst for CO reduction.[21] Inspired by these, the goal of this work is to combine HM-SiO_2, Co−Al LDH, and graphene to improve their toxic effluents capture and elimination effectiveness.

As we known, silica is negatively charged favoring the positively charged coating.[22] Co−Al LDH is a well-investigated member of the LDH family as a result of its ease of synthesis and delamination.[23] The exfoliated single sheets of Co−Al

Received: January 7, 2015
Accepted: April 8, 2015
Published: April 8, 2015

DOI: 10.1021/acsami.5b00176
ACS Appl. Mater. Interfaces 2015, 7, 8506−8514

LDH is positively charged with a thickness of 0.8 nm.[24] Graphene oxide (GO) could be considered as a negatively charged single sheet of graphene, because of the presence of carboxylate.[25] Electrostatic interactions among negatively charged HM-SiO_2, positively charged Co−Al LDH sheets and negatively charged GO could form layered structures on the HM-SiO_2 surface by a self-assembly process.

In this work, a novel sonochemical method was used to prepare HM-SiO_2 without using any templates. Then, HM-SiO_2@Co−Al LDH@graphene was synthesized by self-assembly of CoAl LDH and GO on the HM-SiO_2 surface followed by chemical reduction, as shown in Scheme 1. The HM-SiO_2@Co−Al LDH@graphene hybrids then were added into the EP matrix for investigation of their toxic effluents capture and elimination effectiveness during combustion. It is anticipated that the combination of HM-SiO_2, Co−Al LDH, and graphene could effectively capture and reduce toxic effluents during the combustion of EP.

Scheme 1. Synthetic Route of HM-SiO_2@Co−Al LDH@graphene

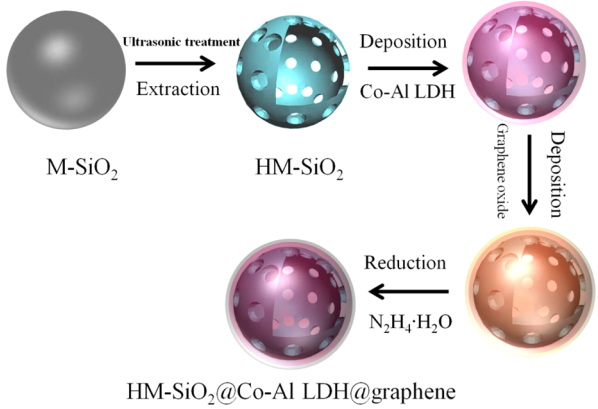

2. EXPERIMENTAL SECTION

2.1. Materials. Tetraethyl orthosilicate (TEOS), cetyltrimethylammonium bromide (CTAB), $Co(NO_3)_2·6H_2O$, $Al(NO_3)_3·9H_2O$, tetrahydrofuran, and 4,4′-diaminodiphenylmethane were obtained from Sinopharm Chemical Reagent Co., Ltd. (Shanghai, China). Bisphenol-A type EP was purchased from Shixian Chemical Industry Co., Ltd. (Guangzhou, China).

2.2. Synthesis of HM-SiO_2. A quantity of 0.35 g of CTAB was dissolved in solution of water (130 mL) and ethanol (600 mL), including 1 mL of $NH_3·H_2O$. Then, 2.08 g of TEOS was added into the above solution at 35 °C. After 24 h of thermostatic reaction, mesoporous silica was obtained by filtration. Then, the white mesoporous silica was dispersed in 100 mL of deionized water through vigorously ultrasonic stirring (see the Supporting Information). After vigorous ultrasonic stirring for 4 h, the product was collected and washed with ethanol. To extract CTAB, the sample was further treated two times with 50 mL of HCl ethanol solution by stirring at 60 °C. The CTAB-extracted HM-SiO_2 was washed with ethanol and dried under high vacuum. The yield of the final HM-SiO_2 was 75%.

2.3. Preparation of HM-SiO_2@Co−Al LDH@graphene by the Self-Assembled Process. HM-SiO_2@Co−Al LDH@graphene was prepared by alternately adsorption Co−Al LDH (see the Supporting Information) and graphene. HM-SiO_2 (0.025 g) was added into the formamide solution of Co−Al LDH (50 mL, 1 mg/mL) by ultrasonication for 20 min. The particles were isolated and washed with deionized water. The obtained HM-SiO_2@Co−Al LDH then was added into the solution of GO (100 mL, 0.2 g/L) by ultrasonication for 20 min. The pink precipitate was collected and named as HM-SiO_2@Co−Al LDH@GO. Finally, HM-SiO_2@Co−Al LDH@graphene was generated by chemical reduction of the aqueous HM-SiO_2@Co−Al LDH@GO dispersion by hydrazine. The HM-SiO_2@Co−Al LDH@graphene hybrids were obtained and dried at 60 °C. The yield of HM-SiO_2@Co−Al LDH@graphene was 85%.

2.4. Preparation of EP/HM-SiO_2@Co−Al LDH@graphene Composite. A quantity of 1 g of HM-SiO_2@Co−Al LDH@graphene

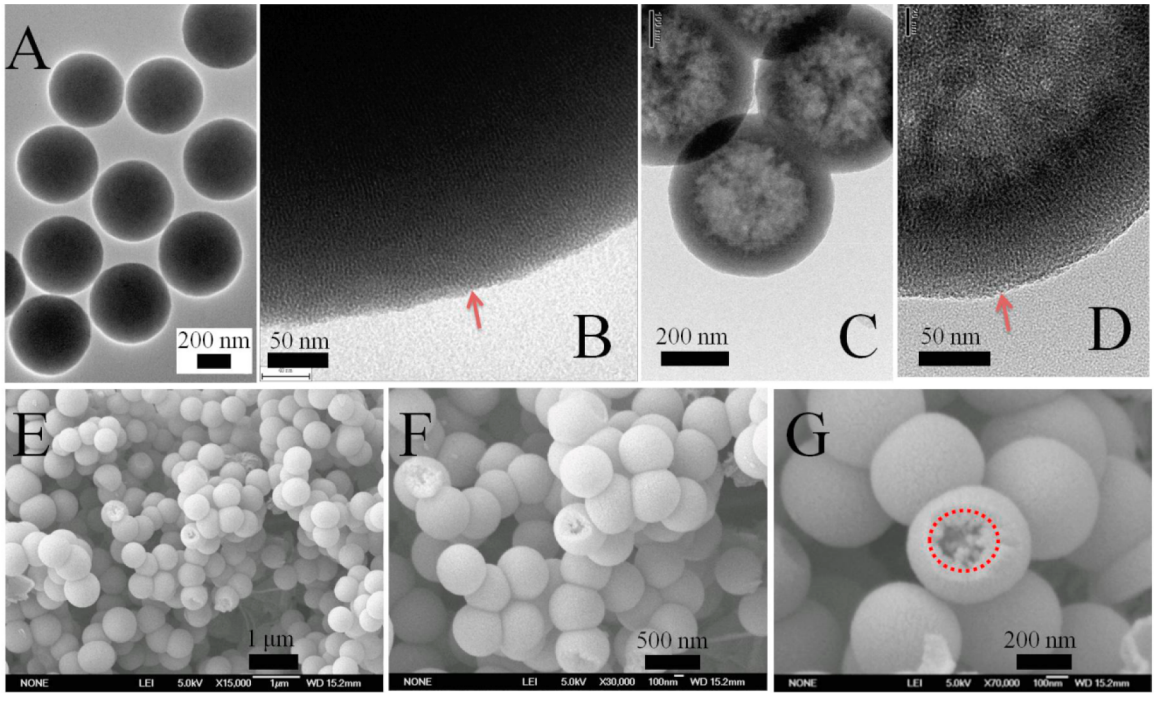

Figure 1. (A, B) TEM images of M-SiO_2; (C, D, E) TEM images of HM-SiO_2; and (F, G) SEM images of HM-SiO_2.

DOI: 10.1021/acsami.5b00176
ACS Appl. Mater. Interfaces 2015, 7, 8506−8514

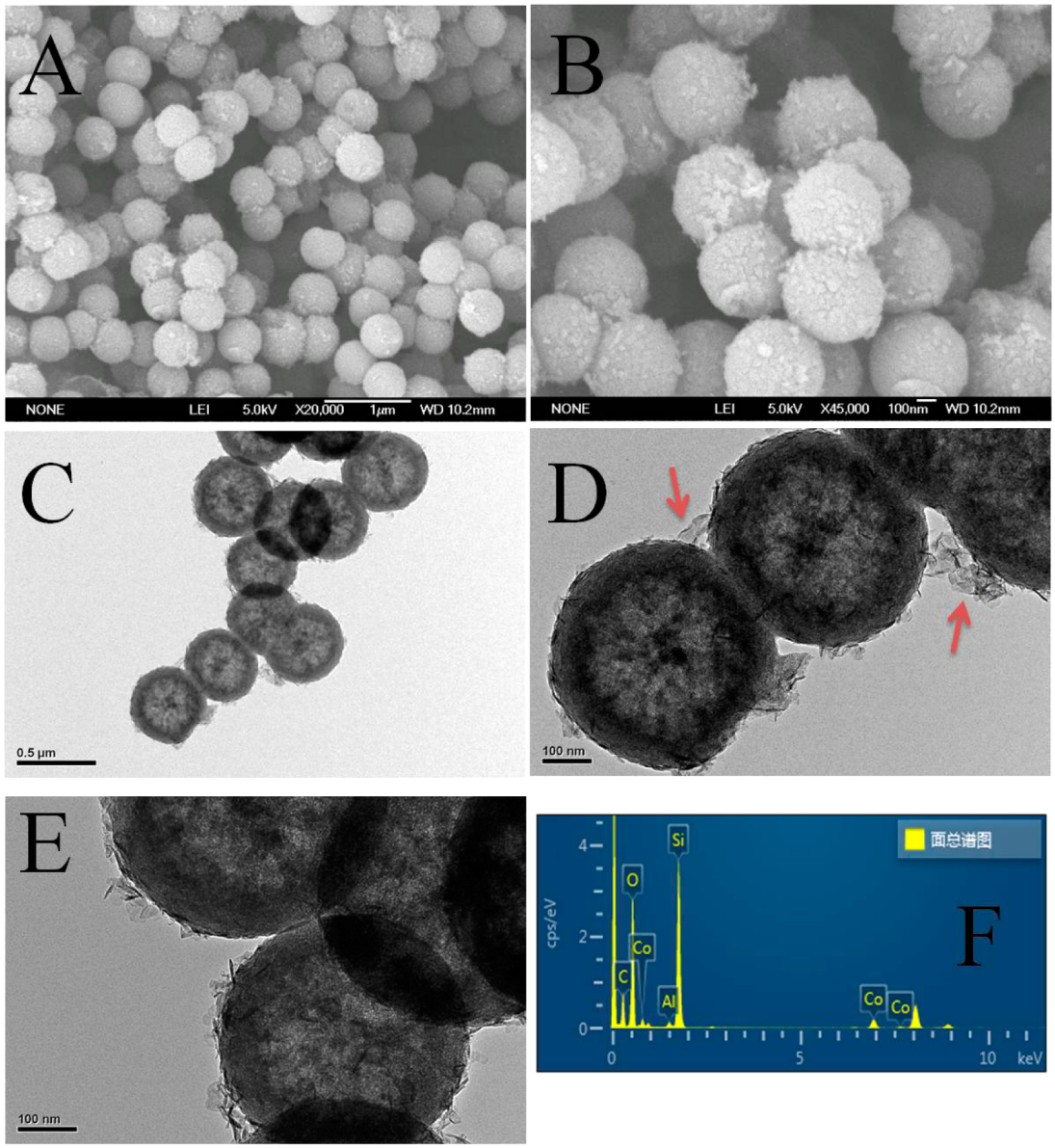

Figure 2. (A, B) SEM images of HM-SiO_2@Co−Al LDH; (C, D, E) TEM images of HM-SiO_2@Co−Al LDH@graphene; and (F) EDX spectrum of HM-SiO_2@Co−Al LDH@graphene.

was dispersed in 50 mL of tetrahydrofuran solution by ultrasonic treatment for 10 min. Then, 41.7 g of EP was added into the above solution with mechanical stirring for 2 h. The white slurry was dried at 60 °C for 12 h in a vacuum oven. Subsequently, 8.3 g of 4,4′-diaminodiphenylmethane was melt and mixed with the above white slurry for 2 min. Finally, EP/HM-SiO_2@Co−Al LDH@graphene was cured at 100 and 150 °C for 2 h, respectively.

2.5. Characterization. X-ray diffraction (XRD) (Model DMax/rA, Rigaku, Japan) was performed using a rotating anode X-ray diffractometer with Cu Kα radiation (λ = 0.154 nm) at 40 kV. Field-emission scanning electron microscopy (SEM) (Model JSM-2010, JEOL) was used to observe the structure of HM-SiO_2 and HM-SiO_2@Co−Al LDH. Transmission electron microscopy (TEM) (Model H-800, Hitachi, Tokyo, Japan) was performed to analyze the morphology and structure of HM-SiO_2 and HM-SiO_2@Co−Al LDH@graphene. Scanning transmission electron microscopy (STEM) (Model JEM 2100F, JEOL) was carried out to characterize the distribution of the elements. X-ray photoelectron spectroscopy (XPS) tests were measured on an ESCALAB MK-II electron spectrometer with a Al Kα X-ray source. Raman spectroscopy measurements were carried out with a SPEX-1403 laser Raman spectrometer (SPEX Co, USA) with excitation provided in backscattering geometry by a 514.5 nm argon laser line. Nitrogen adsorption−desorption isotherms at the temperature of liquid nitrogen were measured with a Micromeritics Coulter (USA) instrument. Thermogravimetric analyzer coupled with Fourier transform infrared spectroscopy (TG-FTIR) was performed using the TGA Q5000 IR thermogravimetric analyzer which was coupled with the Nicolet 6700 FT-IR spectrophotometer via a stainless steel transfer pipe. The fire toxicity was assessed using a steady state tube furnace (SSTF, ISO TS 19700), as reported in previous literature.[26,27]

3. RESULTS AND DISCUSSION

3.1. Characterization of HM-SiO_2@Co−Al LDH@graphene. Figure 1A shows that mesoporous silica spheres are solid and monodispersed with a uniform diameter of ∼500 nm, and they consist of a radially oriented ordered mesostructure (Figure 1B). After ultrasonic treatment for the mesoporous silica spheres, HM-SiO_2 was obtained with the original spherical morphology and size. The contrast between the bright center position and the black edge confirms the hollow interiors

DOI: 10.1021/acsami.5b00176
ACS Appl. Mater. Interfaces 2015, 7, 8506−8514

(Figure 1C). Further magnification (Figure 1D) exhibits that the HM-SiO_2 mesopores are continuous throughout the shell. In the SEM images (Figures 1E, 1F, and 1G), some broken spheres could be observed, which is consistent with TEM observation. Because of these results, we proposed that the generation of the hollow mesoporous structure is due to dissolution of the mesoporous silica. Sonochemical method is a useful technique for the preparation of materials with unique morphology. During the sonication process, the formation, growth, and implosive collapse of bubbles in a liquid can drive many physical and chemical and effects such as accelerating dissolutions of solids, generating emulsions, exfoliating layered materials, oxidation, and reduction.[28−31] When the mesoporous silica spheres were dispersed in the deionized water, the water molecules easily penetrated into the interiors of the mesoporous silica through the mesochannels. Then, the interiors of the mesoporous silica with low condensation degree were readily etched by water under ultrasound treatment.[32,33] Silica species release from the porous silica shells and dissolved in the solution, leading to the formation of the hollow mesoporous structure.

The surface of HM-SiO_2 is negatively charged, confirmed by a zeta potential of −52 mV. Therefore, electrostatic interactions among negatively charged HM-SiO_2, positively charged LDH sheets and negatively charged GO could simply take place without using any surfactant. For HM-SiO_2@Co−Al LDH spheres (Figures 2A and 2B), the spherical morphology is preserved after the assembly of the Co−Al LDH nanosheets. The only remarkable difference is the surface roughness. The morphology of HM-SiO_2@Co−Al LDH@graphene was observed through TEM (Figures 2C, 2D, and 2E). As we have found, the final product has a spherical morphology with a mean size of ∼550 nm. The surface of HM-SiO_2@Co−Al LDH@graphene depicts several layers of curly nanosheets. The presence of Co−Al LDH and graphene on HM-SiO_2 surface was further detected through EDX (see Figure 1F).

The wrinkles of Co−Al LDH and graphene on the HM-SiO_2 surface are further marked in the TEM image of the HM-SiO_2@Co−Al LDH@graphene hybrids by arrows (Figure 3A), confirming that the flexible and ultrathin Co−Al LDH and graphene sheets have indeed successfully encapsulated the HM-SiO_2 spheres. Figure 3B exhibits that the Co−Al LDH with an interlayer distance of 0.8 nm is coated on the HM-SiO_2 surface. In addition, the Co−Al LDH and graphene interface depicts a contact mode of front-back contact. Furthermore, a dark-field STEM analysis of HM-SiO_2@Co−Al LDH@graphene was carried out to characterize the distribution of the elements. Figure 4A shows that HM-SiO_2@Co−Al LDH@graphene has a representative core−shell structure. Furthermore, EDX element mapping of the identical spheres shows the space distribution of Si, O, Co, Al, and C. The intense Si and O signals throughout the spheres confirm the HM-SiO_2 core. Meanwhile, the Co, Al, and C signals examined on the edge distinctly indicate the assembly of the Co−Al LDH and graphene nanosheets.

Figure 5 exhibits the XRD patterns of of HM-SiO_2, Co−Al LDH, graphene, and HM-SiO_2@Co−Al LDH@graphene. The diffraction pattern (Figure 5A) of HM-SiO_2 depicts a reflection characteristic of amorphous silica.[34] After coating with the Co−Al LDH and graphene layers, peaks resulted from Co−Al LDH can be observed beside silica (Figure 5A). Figure 5B shows the small-angle XRD patterns of HM-SiO_2 and HM-SiO_2@Co−Al LDH@graphene. Both curves depict representative reflections

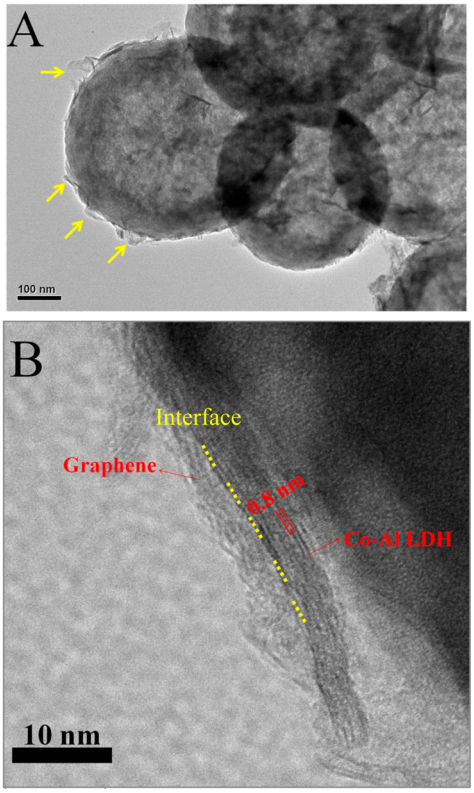

Figure 3. TEM and HRTEM images of HM-SiO_2@Co−Al LDH@graphene.

of hexagonally packed mesopores.[35] Nitrogen adsorption/desorption isotherm of the HM-SiO_2@Co−Al LDH@graphene spheres exhibits a type IV isotherm on the basis of the IUPAC nomenclature (Figure 5C), implying a mesoporous structure with narrow pore-size distribution. The average pore size of HM-SiO_2@Co−Al LDH@graphene is ca. 4.0 nm.

The composition and chemical state of HM-SiO_2 and HM-SiO_2@Co−Al LDH@graphene were investigated using an XPS technique. The XPS survey spectrum of HM-SiO_2@Co−Al LDH@graphene (Figure 6A) shows that the particle includes Si, O, Co, Al, and C elements, implying the generation of HM-SiO_2@Co−Al LDH@graphene. The Co_{2p} spectrum is deconvoluted into Co $2p_{3/2}$ and Co $2p_{1/2}$ located at 781.2 and 796.8 eV. The Co $2p_{3/2}$ peak of HM-SiO_2@Co−Al LDH@graphene centers at higher position than that of Co−Al LDH (Figure 6B), suggesting a strong interaction between HM-SiO_2 and Co−Al LDH.[33−35] Figure 6C shows the Raman spectra of HM-SiO_2 and HM-SiO_2@Co−Al LDH@graphene. For HM-SiO_2, there is no obvious characteristic peak. After electrostatic interaction among HM-SiO_2, Co−Al LDH, and graphene, HM-SiO_2@Co−Al LDH@graphene shows two peaks at 1351 and 1590 cm^{-1}, which are the main features in the Raman spectrum of graphene.[36,37] The 1351 cm^{-1} peak indicates defect structures due to vacancies and amorphous carbon species, while the 1590 cm^{-1} peak is attributable to the E_{2g} phonon of C sp^2 atoms. Combined with the results of XRD, EDX, HRTEM, STEM, XPS and Raman spectra, it is reasonable to believe that the hybrids that included HM-SiO_2, Co−Al LDH, and graphene was successfully synthesized.

3.2. Toxic Effluents Analyzed by SSTF and TG-FTIR. The ISO-TS 19700 SSTF was used to evaluate the yields of toxic combustion products. The CO and hydrocarbons

DOI: 10.1021/acsami.5b00176
ACS Appl. Mater. Interfaces 2015, 7, 8506−8514

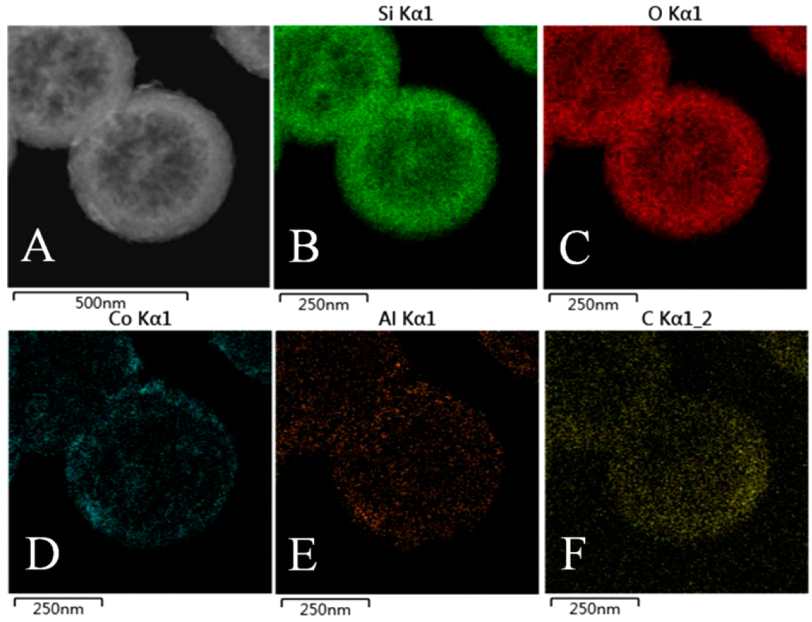

Figure 4. (A) Dark-field STEM image of HM-SiO_2@Co−Al LDH@graphene. Elemental mapping of HM-SiO_2@Co−Al LDH@graphene: (B) Si, (C) O, (D) Co, (E) Al, and (F) C.

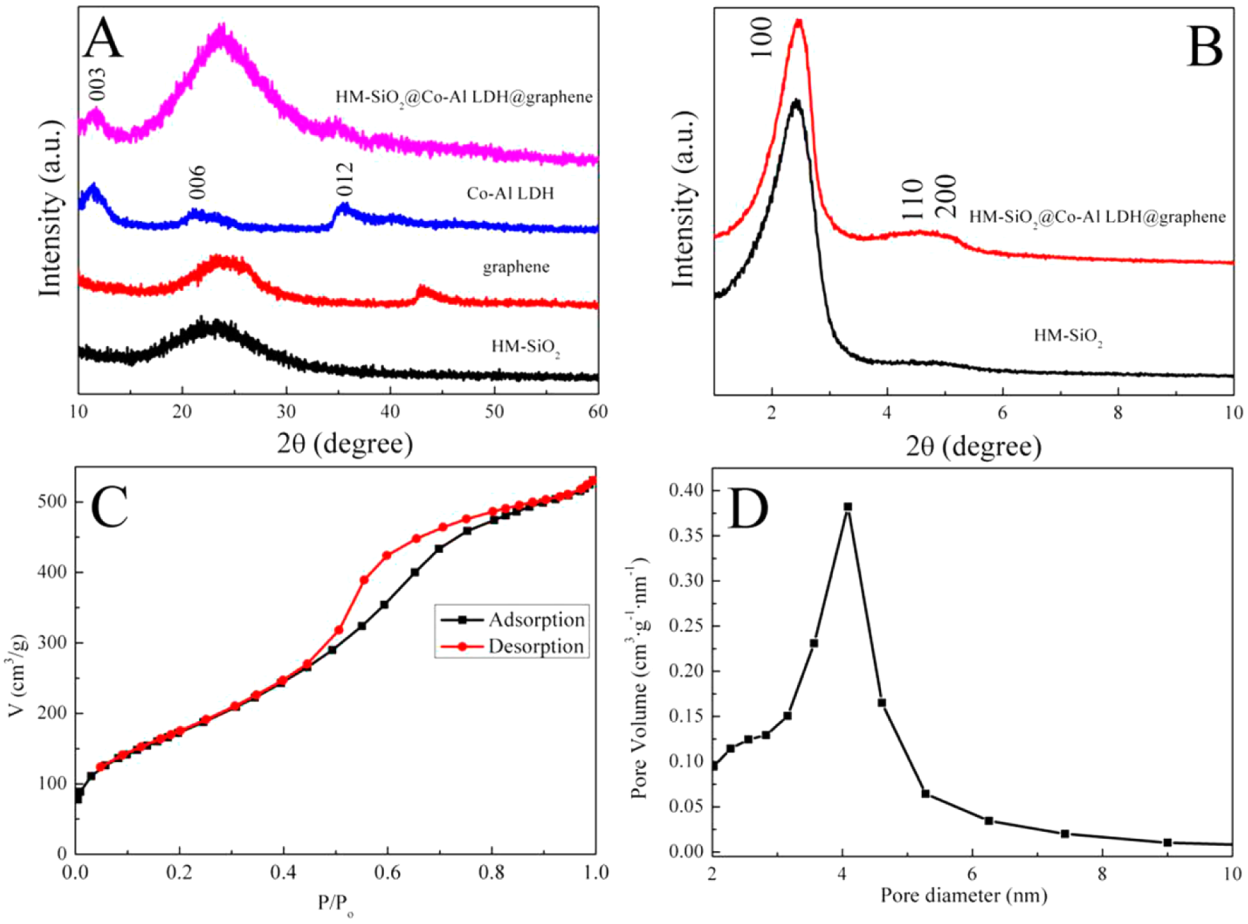

Figure 5. (A) Wide-angle XRD patterns of HM-SiO_2, graphene, Co−Al LDH, and HM-SiO_2@Co−Al LDH@graphene. (B) Low-angle XRD patterns of HM-SiO_2 and HM-SiO_2@Co−Al LDH@graphene. (C) Nitrogen adsorption−desorption isotherm and (D) pore size distribution curve of HM-SiO_2@Co−Al LDH@graphene.

concentrations released from EP and its nanocomposites decomposition are depicted in Figure 7. EP burns very quickly after ignition, the CO and hydrocarbons concentrations reach 1249 and 178 ppm. Hollow or mesoporous silica is usually used

DOI: 10.1021/acsami.5b00176
ACS Appl. Mater. Interfaces 2015, 7, 8506−8514

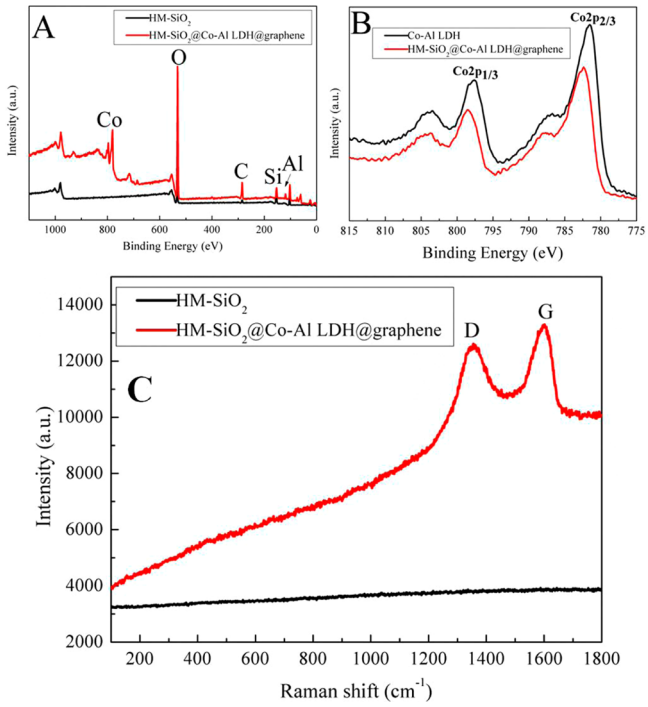

Figure 6. (A) XPS survey spectra of HM-SiO_2 and HM-SiO_2@Co−Al LDH@graphene. (B) Co 2p XPS spectra of Co−Al LDH and HM-SiO_2@Co−Al LDH@graphene. (C) Raman spectra of HM-SiO_2 and HM-SiO_2@Co−Al LDH@graphene.

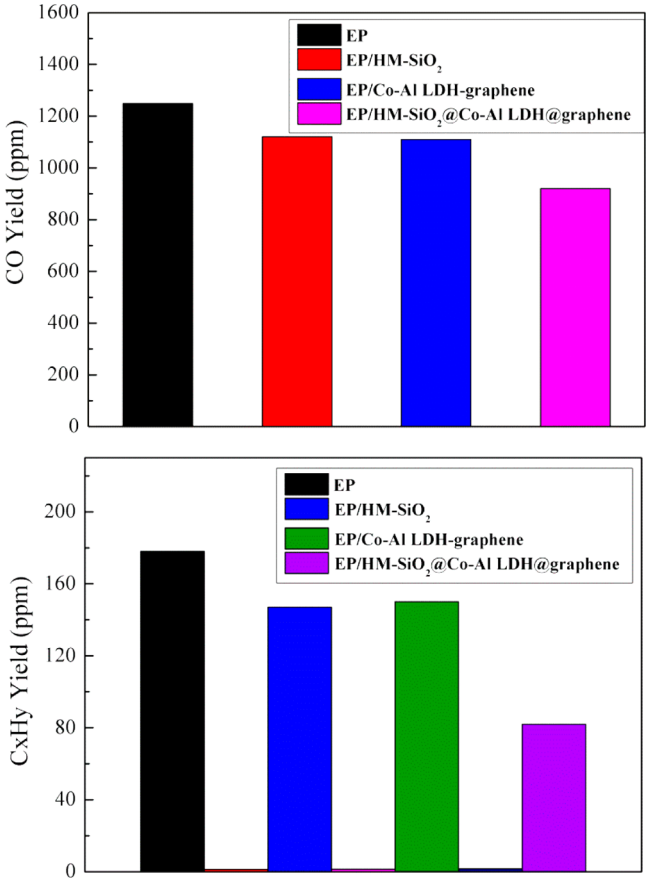

Figure 7. CO and hydrocarbons yields of EP and its nanocomposites.

to remove toxic gases due to its large surface area.[38] As expected, incorporating HM-SiO_2 into EP decreases the CO and hydrocarbons concentrations to 1120 and 147 ppm. For EP/Co−Al LDH-graphene, the CO and hydrocarbons concentrations decrease to 1109 and 150 ppm. In addition, the CO and hydrocarbons concentrations of EP/HM-SiO_2@Co−Al LDH@graphene show further reduction, compared with these of EP/HM-SiO_2 or EP/Co−Al LDH-graphene. The results exhibit that the HM-SiO_2@Co−Al LDH@graphene spheres present the best toxic suppression effect.

To further investigate the capture and elimination behavior of HM-SiO_2@Co−Al LDH@graphene, the toxic gases released from EP and EP/HM-SiO_2@Co−Al LDH@graphene decomposition were monitored by using a TG-FTIR technique. 3D TG-FTIR and FTIR spectra obtained at the maximum evolution rate during the thermal decomposition of EP and EP/HM-SiO_2@Co−Al LDH@graphene are shown in Figure 8. Some toxic gaseous decomposition products are unambiguously identified by characteristic strong FTIR signals, such as hydrocarbons (3100−2800 cm^{-1}) and aromatic compounds (1605, 1510, and 1460 cm^{-1}).

In order to make a comparison, the intensities of representative gaseous products for neat EP and EP/HM-SiO_2@Co−Al LDH@graphene composite are presented in Figure 9. With the incorporation of HM-SiO_2@Co−Al LDH@graphene, the intension of toxic gases emission is shifted to lower values, containing hydrocarbons, aromatic compounds, and CO. The organic compounds removed further leads to the suppression of smoke, due to that the hydrocarbons and aromatic compounds can aggregate to generate smoke. Moreover, the elimination of gaseous volatiles can dramatically reduce the degradation products toxicity.

3.3. Toxic Effluents Capture and Elimination Mechanism. The plausible mechanism was proposed for the reduced toxicity of EP/HM-SiO_2@Co−Al LDH@graphene. On one hand, the metal catalysis has been reported to be an effective method to eliminate toxic compounds during combustion reactions.[39,40] As an important functional metal element, Co species have exciting catalytic effects, because of their distinctive physical and chemical properties. Xie et al. found that Co_3O_4 was a catalyst with great promise in CO oxidation.[41] Research conducted by Li et al. demonstrated that Co_3O_4 exhibited excellent catalytic ability for the removal of organic volatiles.[42] Moreover, the presence of graphene can improve the catalytic ability of Co species.[43,44] Therefore, it is reasonably believed that the catalytic effect of the combination of Co−Al LDH and graphene plays a key role in the elimination of toxic gases. On the other hand, hollow and mesoporous silicas have great potential for the removal of volatile organic compounds due to their large surface area and high porosity.[38] The large surface area is in favor of the adsorption of bulky molecules. In previous studies, different type mesoporous silicas have been used as adsorbents for the volatile organic compounds removal.[45,46] Meanwhile, it is well-known that the silanol groups (Si−OH) on the pore surfaces act as the adsorption sites for various molecules by weak π-system hydrogen bonding with silanols on the silica surface.[47,48] Therefore, HM-SiO_2 played a role in the capture of toxic effluents. Furthermore, the synergistic effects between Co−Al LDH and silica can promote char formation in the EP nanocomposites (see the Supporting Information),[49] which can restrain the release of the gaseous volatiles.[26] Overall, synergistic effect from respective components (Co−Al LDH and graphene) plus the HM-SiO_2 spheres

DOI: 10.1021/acsami.5b00176
ACS Appl. Mater. Interfaces 2015, 7, 8506−8514

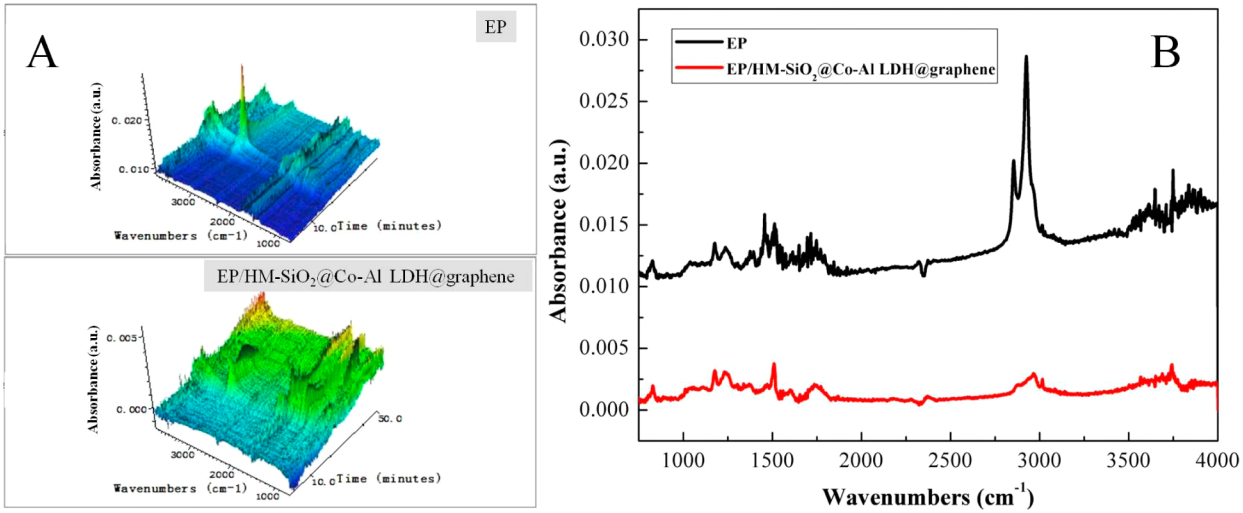

Figure 8. (A) Three-dimensional (3D) TG-FTIR spectra of gasified pyrolysis products for pure EP and EP/HM-SiO_2@Co−Al LDH@graphene. (B) FTIR spectra of gasified pyrolysis products for pure EP and EP/HM-SiO_2@Co−Al LDH@graphene at the maximum evolution rate.

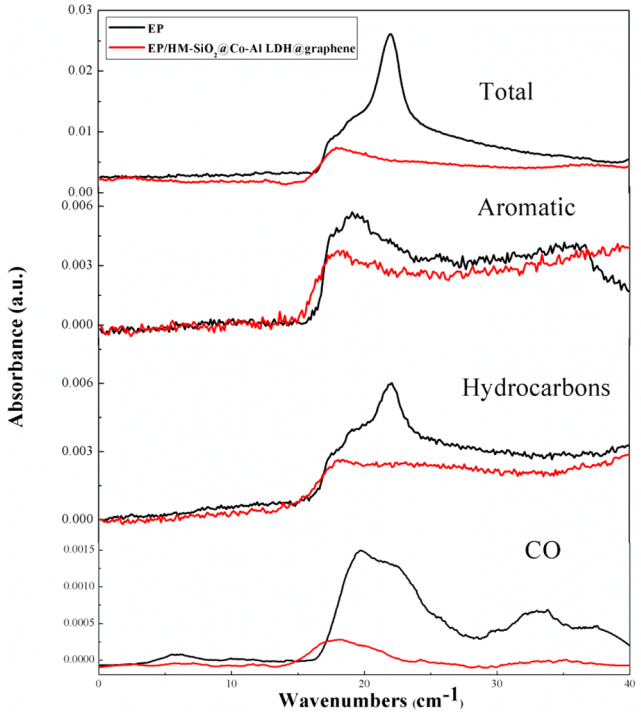

Figure 9. Intensity of characteristic peaks for pyrolysis products of pure EP and EP/HM-SiO_2@Co−Al LDH@graphene nanocomposite.

offers the hybrid a superior toxic effluents elimination performance. The reduction of fire effluents will be beneficial to fire rescue when an accident happens.

4. CONCLUSION

A simple and effective sonochemical way was used to prepare hollow mesoporous silica without using any templates. Then, HM-SiO_2@Co−Al LDH@graphene spheres were prepared by self-assembly of Co−Al LDH and GO on the HM-SiO_2 surface. After electrostatic assembly and chemical reduction, the HM-SiO_2 spheres were intimately encapsulated by the ultrathin Co−Al LDH and graphene. Subsequently, the HM-SiO_2@Co−Al LDH@graphene spheres were added into the epoxy resin (EP) matrix to study their toxic effluents capture and elimination effectiveness during combustion. SSTF and TG-FTIR results indicated that the combination of HM-SiO_2, Co−Al LDH, and graphene could effectively capture and eliminate toxic gases during the combustion of EP.

■ ASSOCIATED CONTENT

Supporting Information

Supporting Information include: (i) synthesis of Co−Al LDH; (ii) supplementary figures with discussion that is not mentioned in the main text; and (iii) references that are cited in the Supporting Information. This material is available free of charge via the Internet at http://pubs.acs.org/.

■ AUTHOR INFORMATION

Corresponding Author

*Tel.: 86 551 63601664. Fax: 86 551 63601664. E-mail: yuanhu@ustc.edu.cn.

Notes

The authors declare no competing financial interest.

■ ACKNOWLEDGMENTS

The work was financially supported by the National Basic Research Program of China (973 Program) (NO. 2012CB719701), the National Natural Science Foundation of China (21374111), the National Natural Science Foundation of China (51303165), and China Postdoctoral Science Foundation (No. 2014M561838).

■ REFERENCES

(1) Gu, H. B.; Guo, J.; He, Q. L.; Tadakamalla, S.; Zhang, X.; Yan, X. R.; Huang, Y. D.; Colorado, H. A.; Wei, S. Y.; Guo, Z. H. Flame-Retardant Epoxy Resin Nanocomposites Reinforced with Polyaniline-Stabilized Silica Nanoparticles. *Ind. Eng. Chem. Res.* **2013**, *52*, 7718−7728.

(2) Wang, X.; Song, L.; Yang, H. Y.; Xing, W. Y.; Kandola, B.; Hua, Y. Simultaneous Reduction and Surface Functionalization of Graphene Oxide with POSS for Reducing Fire Hazards in Epoxy Composites. *J. Mater. Chem.* **2012**, *22*, 22037−22043.

(3) Wang, X.; Zhou, S.; Xing, W. Y.; Yu, B.; Feng, X. M.; Song, L.; Hu, Y. Self-Assembly of Ni-Fe Layered Double Hydroxide/Graphene Hybrids for Reducing Fire Hazard in Epoxy Composites. *J. Mater. Chem. A* **2013**, *1*, 4383−4390.

DOI: 10.1021/acsami.5b00176
ACS Appl. Mater. Interfaces 2015, 7, 8506−8514

(4) Jin, W. Q.; Yuan, L.; Liang, G. Z.; Gu, A. J. Multifunctional Cyclotriphosphazene/Hexagonal Boron Nitride Hybrids and Their Flame Retarding Bismaleimide Resins with High Thermal Conductivity and Thermal Stability. *ACS Appl. Mater. Interfaces* **2014**, *6*, 14931−14944.
(5) Chen, Y.; Chen, H. R.; Shi, J. L. Construction of Homogenous/Heterogeneous Hollow Mesoporous Silica Nanostructures by Silica-Etching Chemistry: Principles, Synthesis, and Applications. *Acc. Chem. Res.* **2014**, *47*, 125−137.
(6) Wang, S. N.; Zhang, M. C.; Zhang, W. Q. Yolk−Shell Catalyst of Single Au Nanoparticle Encapsulated within Hollow Mesoporous Silica Microspheres. *ACS Catal.* **2011**, *1*, 207−211.
(7) Fang, X. L.; Zhao, X. J.; Fang, W. J.; Chen, C.; Zheng, N. F. Self-Templating Synthesis of Hollow Mesoporous Silica and Their Applications in Catalysis and Drug Delivery. *Nanoscale* **2013**, *5*, 2205−2218.
(8) Schacht, S.; Huo, Q.; VoigtMartin, I. G.; Stucky, G. D.; Schuth, F. Oil−Water Interface Templating of Mesoporous Macroscale Structures. *Science* **1996**, *273*, 768−771.
(9) Wang, J. G.; Xiao, Q.; Zhou, H. J.; Sun, P. C.; Yuan, Z. Y.; Li, B. H.; Ding, D. T.; Shi, A. C.; Chen, T. H. Budded, Mesoporous Silica Hollow Spheres: Hierarchical Structure Controlled by Kinetic Self-Assembly. *Adv. Mater.* **2006**, *18*, 3284−3288.
(10) Chen, Y.; Chen, H. R.; Guo, L. M.; He, Q. J.; Chen, F.; Zhou, J.; Feng, J. W.; Shi, J. L. Hollow/Rattle-Type Mesoporous Nanostructures by a Structural Difference-Based Selective Etching Strategy. *ACS Nano* **2010**, *4*, 529−539.
(11) Chen, J.; Wu, X.; Hou, X.; Su, X.; Chu, Q.; Fahruddin, N.; Zhao, J. X. Shape-Tunable Hollow Silica Nanomaterials Based on a Soft-Templating Method and Their Application as a Drug Carrier. *ACS Appl. Mater. Interfaces* **2014**, *6*, 21921−21930.
(12) Gao, T.; Jelle, B. P.; Sandberg, L. I.; Gustavsen, A. Monodisperse Hollow Silica Nanospheres for Nano Insulation Materials: Synthesis, Characterization, and Life Cycle Assessment. *ACS Appl. Mater. Interfaces* **2013**, *5*, 761−767.
(13) He, Q. L.; Yuan, T. T.; Wei, S. Y.; Haldolaarachchige, N.; Luo, Z. P.; Young, D. P.; Khasanov, A.; Guo, Z. H. Morphology- and Phase-Controlled Iron Oxide Nanoparticles Stabilized with Maleic Anhydride Grafted Polypropylene. *Angew. Chem., Int. Ed.* **2012**, *51*, 8842−8845.
(14) He, Q. L.; Yuan, T. T.; Luo, Z. P.; Haldolaarachchige, N.; Young, D. P.; Wei, S. Y.; Guo, Z. H. Morphology and Phase Controlled Cobalt Nanostructures in Magnetic Polypropylene Nanocomposites: The Role of Alkyl Chain-Length in Maleic Anhydride Grafted Polypropylene. *Chem. Commun.* **2013**, *49*, 2679−2681.
(15) Zhang, X.; Alloul, O.; Zhu, J. H.; He, Q. L.; Luo, Z. P.; Colorado, H. A.; Haldolaarachchige, N.; Young, D. P.; Shen, T. D.; Wei, S. Y.; Guo, Z. H. Iron-Core Carbon-Shell Nanoparticles Reinforced Electrically Conductive Magnetic Epoxy Resin Nanocomposites with Reduced Flammability. *RSC Adv.* **2013**, *3*, 9453−9464.
(16) Gu, H. B.; Guo, J.; Zhang, X.; He, Q. L.; Huang, Y. D.; Colorado, H. A.; Haldolaarachchige, N.; Xin, H. L.; Young, D. P.; Wei, S. Y.; Guo, Z. H. Giant Magnetoresistive Phosphoric Acid Doped Polyaniline−Silica Nanocomposites. *J. Phys. Chem. C* **2013**, *117*, 6426−6436.
(17) Li, X. M.; Zhou, L.; Wei, Y.; El-Toni, A. M.; Zhang, F.; Zhao, D. Y. Anisotropic Growth-Induced Synthesis of Dual-Compartment Janus Mesoporous Silica Nanoparticles for Bimodal Triggered Drugs Delivery. *J. Am. Chem. Soc.* **2014**, *136*, 15086−15092.
(18) Shao, M. F.; Ning, F. Y.; Zhao, J. W.; Wei, M.; Evans, D. G.; Duan, X. Preparation of Fe_3O_4@SiO_2@Layered Double Hydroxide Core−Shell Microspheres for Magnetic Separation of Proteins. *J. Am. Chem. Soc.* **2012**, *134*, 1071−1077.
(19) Rezlescu, N.; Rezlescu, E.; Popa, P. D.; Doroftei, C.; Ignat, M. Scandium Substituted Nickel−Cobalt Ferrite Nanoparticles for Catalyst Applications. *Appl. Catal., B* **2014**, *158*, 70−75.
(20) Xie, X. W.; Li, Y.; Liu, Z. Q.; Haruta, M.; Shen, W. J. Low-Temperature Oxidation of CO Catalysed by Co_3O_4 Nanorods. *Nature* **2009**, *458*, 746−749.
(21) Wang, X.; Song, L.; Yang, H. Y.; Xing, W. Y.; Lu, H. D.; Hu, Y. Cobalt Oxide/Graphene Composite for Highly Efficient CO Oxidation and Its Application in Reducing the Fire Hazards of Aliphatic Polyesters. *J. Mater. Chem.* **2012**, *22*, 3426−3431.
(22) Zhu, Y. F.; Shi, J. L.; Shen, W. H.; Dong, X. P.; Feng, J. W.; Ruan, M. L.; Li, Y. S. Stimuli-Responsive Controlled Drug Release from a Hollow Mesoporous Silica Sphere/Polyelectrolyte Multilayer Core−Shell Structure. *Angew. Chem., Int. Ed.* **2005**, *44*, 5083−5087.
(23) Wu, Q. L.; Olafsen, A.; Vistad, O. B.; Roots, J.; Norby, P. Delamination and Restacking of a Layered Double Hydroxide with Nitrate as Counter Anion. *J. Mater. Chem.* **2005**, *15*, 4695−4700.
(24) Wang, L.; Wang, D.; Dong, X. Y.; Zhang, Z. J.; Pei, X. F.; Chen, X. J.; Chen, B. A.; Jin, J. A. Layered Assembly of Graphene Oxide and Co-Al Layered Double Hydroxide Nanosheets as Electrode Materials for Supercapacitors. *Chem. Commun.* **2011**, *47*, 3556−3558.
(25) Dreyer, D. R.; Park, S.; Bielawski, C. W.; Ruoff, R. S. The Chemistry of Graphene Oxide. *Chem. Soc. Rev.* **2010**, *39*, 228−240.
(26) Jiang, S. D.; Bai, Z. M.; Tang, G.; Song, L.; Stec, A. A.; Hull, T. R.; Zhan, J.; Hu, Y. Fabrication of Ce-Doped MnO_2 Decorated Graphene Sheets for Fire Safety Applications of Epoxy Composites: Flame Retardancy, Smoke Suppression and Mechanism. *J. Mater. Chem. A* **2014**, *2*, 17341−17351.
(27) Stec, A. A.; Hull, T. R.; Lebek, K. Characterisation of the Steady State Tube Furnace (ISO TS 19700) for Fire Toxicity Assessment. *Polym. Degrad. Stab.* **2008**, *93*, 2058−2065.
(28) Pinkas, J.; Reichlova, V.; Serafimidisova, A.; Moravec, Z.; Zboril, R.; Jancik, D.; Bezdicka, P. Sonochemical Synthesis of Amorphous Yttrium Iron Oxides Embedded in Acetate Matrix and their Controlled Thermal Crystallization toward Garnet ($Y_3Fe_5O_{12}$) and Perovskite ($YFeO_3$) Nanostructures. *J. Phys. Chem. C* **2010**, *114*, 13557−13564.
(29) Pinkas, J.; Reichlova, V.; Zboril, R.; Moravec, Z.; Bezdicka, P.; Matejkova, J. Sonochemical Synthesis of Amorphous Nanoscopic Iron(III) Oxide from $Fe(acac)_3$. *Ultrason. Sonochem.* **2008**, *15*, 257−264.
(30) Coskuner, B.; Figen, A. K.; Piskin, S. Sonochemical Approach to Synthesis of Co-B Catalysts and Hydrolysis of Alkaline $NaBH_4$ Solutions. *J. Chem.* **2014**, *2014*, 185957.
(31) Xu, H. X.; Zeiger, B. W.; Suslick, K. S. Sonochemical Synthesis of Nanomaterials. *Chem. Soc. Rev.* **2013**, *42*, 2555−2567.
(32) Gunnarsson, I.; Arnorsson, S. Amorphous Silica Solubility and the Thermodynamic Properties of $H_4SiO_4^\circ$ in the Range of 0° to 350 °C at P_{sat}. *Geochim. Cosmochim. Acta* **2000**, *64*, 2295−2307.
(33) Alexander, G. B.; Heston, W. M.; Iler, R. K. The Solubility of Amorphous Silica in Water. *J. Phys. Chem.* **1954**, *58*, 453−455.
(34) Yan, N.; Wang, F.; Zhong, H.; Li, Y.; Wang, Y.; Hu, L.; Chen, Q. W. Hollow Porous SiO_2 Nanocubes Towards High-Performance Anodes for Lithium-ion Batteries. *Sci. Rep.* **2013**, *3*, 1568.
(35) Kresge, C. T.; Leonowicz, M. E.; Roth, W. J.; Vartuli, J. C.; Beck, J. S. Ordered Mesoporous Molecular-Sieves Synthesized by a Liquid-Crystal Template Mechanism. *Nature* **1992**, *359*, 710−712.
(36) Dresselhaus, M. S.; Jorio, A.; Hofmann, M.; Dresselhaus, G.; Saito, R. Perspectives on Carbon Nanotubes and Graphene Raman Spectroscopy. *Nano Lett.* **2010**, *10*, 751−758.
(37) Ferrari, A. C. Raman Spectroscopy of Graphene and Graphite: Disorder, Electron-Phonon Coupling, Doping and Nonadiabatic Effects. *Solid State Commun.* **2007**, *143*, 47−57.
(38) Wang, H. N.; Tang, M.; Han, L.; Cao, J. Y.; Zhang, Z. H.; Huang, W. W.; Chen, R. Y.; Yu, C. Z. Synthesis of Hollow Organosiliceous Spheres for Volatile Organic Compound Removal. *J. Mater. Chem. A* **2014**, *2*, 19298−19307.
(39) Sanz, O.; Delgado, J. J.; Navarro, P.; Arzamendi, G.; Gandia, L. M.; Montes, M. VOCs Combustion Catalysed by Platinum Supported on Manganese Octahedral Molecular Sieves. *Appl. Catal., B* **2011**, *110*, 231−237.
(40) Yu, D. Q.; Liu, Y.; Wu, Z. B. A. Low-Temperature Catalytic Oxidation of Toluene over Mesoporous MnO_x−CeO_2/TiO_2 Prepared by Sol−Gel Method. *Catal. Commun.* **2010**, *11*, 788−791.
(41) Zhang, C.; Han, L.; Liu, W.; Yang, H. X.; Zhang, X. Y.; Liu, X. F.; Yang, Y. Z. Facile Synthesis of Novel MnO_x Nano-Structures and

DOI: 10.1021/acsami.5b00176
ACS Appl. Mater. Interfaces 2015, 7, 8506−8514

Their Catalytic Performance on CO Oxidation. *CrystEngComm* **2013**, *15*, 5150−5155.
(42) Zhu, Z. Z.; Lu, G. Z.; Zhang, Z. G.; Guo, Y.; Guo, Y. L.; Wang, Y. Q. Highly Active and Stable Co_3O_4/ZSM-5 Catalyst for Propane Oxidation: Effect of the Preparation Method. *ACS Catal.* **2013**, *3*, 1154−1164.
(43) Sun, Y.; Liu, Q.; Gao, S.; Cheng, H.; Lei, F.; Sun, Z.; Jiang, Y.; Su, H.; Wei, S.; Xie, Y. Pits Confined in Ultrathin Cerium(IV) Oxide for Studying Catalytic Centers in Carbon Monoxide Oxidation. *Nat. Commun.* **2013**, *4*, 2899.
(44) Larachi, F.; Pierre, J.; Adnot, A.; Bernis, A. Ce 3d XPS Study of Composite $Ce_xMn_{1-x}O_{2-y}$ Wet Oxidation Catalysts. *Appl. Surf. Sci.* **2002**, *195*, 236−250.
(45) Serna-Guerrero, R.; Sayari, A. Applications of Pore-Expanded Mesoporous Silica. 7. Adsorption of Volatile Organic Compounds. *Environ. Sci. Technol.* **2007**, *41*, 4761−4766.
(46) Kosuge, K.; Kubo, S.; Kikukawa, N.; Takemori, M. Effect of Pore Structure in Mesoporous Silicas on VOC Dynamic Adsorption/Desorption Performance. *Langmuir* **2007**, *23*, 3095−3102.
(47) Hernandez, M. A.; Velasco, J. A.; Asomoza, M.; Solis, S.; Rojas, F.; Lara, V. H.; Portillo, R.; Salgado, M. A. Alkane Adsorption on Microporous SiO_2 Substrata. 1. Textural Characterization and Equilibrium. *Energy Fuels* **2003**, *17*, 262−270.
(48) Serrano, D. P.; Calleja, G.; Botas, J. A.; Gutierrez, F. J. Adsorption and Hydrophobic Properties of Mesostructured MCM-41 and SBA-15 Materials for Volatile Organic Compound Removal. *Ind. Eng. Chem. Res.* **2004**, *43*, 7010−7018.
(49) Jiang, S. D.; Bai, Z. M.; Tang, G.; Song, L.; Stec, A. A.; Hull, T. R.; Hu, Y.; Hu, W. Z. Synthesis of Mesoporous Silica@Co-Al Layered Double Hydroxide Spheres: Layer-by-Layer Method and Their Effects on the Flame Retardancy of Epoxy Resins. *ACS Appl. Mater. Interfaces* **2014**, *6*, 14076−14086.

DOI: 10.1021/acsami.5b00176
ACS Appl. Mater. Interfaces 2015, 7, 8506−8514